Received 27 November 2021
Revised 19 March 2022
4 May 2022
Accepted 26 May 2022

Combining artificial intelligence and building engineering technologies towards energy efficiency: the case of ventilated façades

Serena Summa
Department of Industrial Engineering and Mathematical Sciences, Universita Politecnica delle Marche Facolta di Ingegneria, Ancona, Italy

Alex Mircoli and Domenico Potena
Department of Information Engineering, Universita Politecnica delle Marche Facolta di Ingegneria, Ancona, Italy

Giulia Ulpiani
Department of Industrial Engineering and Mathematical Sciences, Universita Politecnica delle Marche Facolta di Ingegneria, Ancona, Italy

Claudia Diamantini
Department of Information Engineering, Universita Politecnica delle Marche Facolta di Ingegneria, Ancona, Italy, and

Costanzo Di Perna
Department of Industrial Engineering and Mathematical Sciences, Universita Politecnica delle Marche Facolta di Ingegneria, Ancona, Italy

Abstract

Purpose – Nearly 75% of EU buildings are not energy-efficient enough to meet the international climate goals, which triggers the need to develop sustainable construction techniques with high degree of resilience against climate change. In this context, a promising construction technique is represented by ventilated façades (VFs). This paper aims to propose three different VFs and the authors define a novel machine learning-based approach to evaluate and predict their energy performance under different boundary conditions, without the need for expensive on-site experimentations

Design/methodology/approach – The approach is based on the use of machine learning algorithms for the evaluation of different VF configurations and allows for the prediction of the temperatures in the cavities and of the heat fluxes. The authors trained different regression algorithms and obtained low prediction errors,

Construction Innovation
Vol. 24 No. 7, 2024
pp. 44-64
Emerald Publishing Limited
1471-4175
DOI 10.1108/CI-11-2021-0229

in particular for temperatures. The authors used such models to simulate the thermo-physical behavior of the VFs and determined the most energy-efficient design variant.

Findings – The authors found that regression trees allow for an accurate simulation of the thermal behavior of VFs. The authors also studied feature weights to determine the most relevant thermo-physical parameters. Finally, the authors determined the best design variant and the optimal air velocity in the cavity.

Originality/value – This study is unique in four main aspects: the thermo-dynamic analysis is performed under different thermal masses, positions of the cavity and geometries; the VFs are mated with a controlled ventilation system, used to parameterize the thermodynamic behavior under stepwise variations of the air inflow; temperatures and heat fluxes are predicted through machine learning models; the best configuration is determined through simulations, with no onerous *in situ* experimentations needed.

Keywords Ventilated façades, Machine learning, Temperature prediction, Climate change, Experimental study

Paper type Research paper

1. Introduction

In recent years, the increased attention for environmental issues has emphasized the need for reducing global energy consumption and carbon dioxide (CO_2) emissions (European Parliament, 2018). Nearly 75% of the EU building stock is not efficient enough from an energy perspective (European Parliament, 2012) which calls for energy-efficient, energy-flexible and sustainable construction techniques, with a high degree of resilience against climate change to meet international climate goals and decarbonize the built environment by 2050. In this context, the Directive 2018/844/EU (European Parliament and Council of the European Union, 2018) listed possible actions to be undertaken by member states in order to bring CO_2 emissions to zero:

- energy efficiency of the building envelope for new and existing buildings;
- use of innovative building materials and solutions;
- microclimate control;
- use of high-efficiency electric heat pumps or other carbon-free systems; and
- intelligent controls and digitalization.

With regard to the first action, several passive techniques are documented in the literature that can reduce CO_2 emissions, such as increasing the thermal inertia, providing thermal storage via phase change materials (PCM), adjusting the level of thermal insulation based on the local context and harnessing the potential of natural ventilation and night cooling.

Each technique comes with a suite of advantages: buildings with a high thermal mass are particularly useful in hot-dry regions (Meir and Roaf, 2002) and can reduce the number of hours of discomfort during the summer season by up to 40% (Kumar *et al.*, 2018) by phase-shifting the penetration of the heatwave through the envelope. The use of PCMs, which can store and release a large amount of thermal energy depending on their phase change (Kenisarin and Mahkamov, 2007), allows to passively heat and/or cool environments by peak-shaving, as discussed in Cabeza *et al.* (2007) and Gholamibozanjani and Farid (2020). Thermal insulation is another good solution to reduce the size of the air conditioning system and prevent heat losses in cold locations, leading to reductions of CO_2 emissions by up to 50% (Rahiminejad and Khovalyg, 2021). Finally, natural and night ventilation, if correctly integrated with the building typology, are beneficial both in terms of summer energy savings and thermal comfort (Rahiminejad and Khovalyg, 2021).

A novel and promising construction technique that can be used to reduce CO_2 emissions is represented by ventilated façades (VFs), which were recently proposed and tested as an

alternative to standard façades. A typical VF is a building element that is fixed to the external surface of the envelope by mechanical anchors and through which outside air can flow via openings located at the top and the bottom (Ibañez-Puy *et al.*, 2017; Bikas *et al.*, 2017).

As demonstrated by several studies, the use of VFs can significantly reduce winter and summer energy consumption of buildings (Stazi *et al.*, 2020; Aelenei *et al.*, 2005; Ciampi *et al.*, 2003; Marinosci *et al.*, 2014) as well as guarantee greater durability of the cladding. In fact, the in-cavity ventilation allows for faster evaporation of the water absorbed by the porous coatings, resulting in a significant humidity reduction (Straube and Finch, 2007; Falk and Sandin, 2013a; Vanpachtenbeke *et al.*, 2017).

These aspects are extremely important and have motivated researchers to study these systems trying to determine the optimal configurations according to different types of external coating, climate and air velocities in the ventilated cavity. Since testing several different configurations is very onerous, many studies are based on empirical approaches (Bassett and McNeil, 2005; Falk and Sandin, 2013b), theoretical calculations (Van Straaten *et al.*, 2016; Lorente and Mattias, 1998) and numerical analysis (Francés *et al.*, 2013) especially computational fluid dynamics (CFD) simulations (Gagliano *et al.*, 2016; Gagliano and Aneli, 2020; Patania *et al.*, 2010; Piñon *et al.*, 2004). As highlighted by Rahiminejad and Khovalyg (2021), each of these methods shows some criticalities:

- empirical models tend to be case-specific with little room for generalization;
- theoretical calculations have limited accuracy, may require specific measurements and supply little information about parameters distribution; and
- numerical analysis better depicts the parameters distribution but typically exhibits lower accuracy, but in the case of computationally onerous models like CFD heavily reliant on the user expertise and requiring proper experimental validation.

Therefore, there is the need for an alternative method that may combine the advantage of realistic measurements (as in an *in situ* experimentation) with the possibility of varying the boundary conditions (in our case, the air velocity in the cavity) as in a CFD simulation. In this regard, the use of machine learning algorithms for the simulation of different boundary conditions represents an opportunity that has not yet been sufficiently investigated in the literature. In fact, to the best of our knowledge, no previous research applies machine learning algorithms to VFs and only a few authors focused on the use of supervised learning algorithms for the estimation of the hygrothermal properties of walls. Aznar *et al.* (2018) modeled the thermal behavior of a wall using both traditional techniques and deep learning techniques and found that the latter offers a better approximation of the energy behavior. Sha *et al.* (2021) proposed the use of the gradient tree boosting algorithm for energy modeling in the presence of mechanical ventilation systems.

For this reason, in this paper, three different VF configurations integrated into a mechanical ventilation system are experimentally investigated under varying air velocities inside the cavities to create a suitable data set to be analyzed through machine learning techniques.

Among the proposed VFs, the most innovative one is designed with the purpose of combining the advantages of:

- replacing multilayer assemblies with a monolayer structure that uses cement-bonded wood fiber blocks' air gaps as ventilated cavities; and
- having an easy-to-implement and cost-saving design, notably regarding the details of the metallic support.

The novel design variant is compared with two heavyweight, multilayered designs, already investigated elsewhere (Stazi *et al.*, 2020), that differ in the position of the massive layer with respect to the ventilated cavity.

This study aims to develop a suite of machine learning models that may allow to perform a thermo-physical analysis of the design variants under equal boundary conditions and under the influence of mechanically-controlled cavity ventilation, without the need for extensive on-site experimentations. The goal is to delve into the dynamic response of envelope and indoors with regards to outdoor forcing, in-cavity forcing and wall typology.

Compared to other research lines on VFs, this study is unique in four main aspects:

(1) the thermo-dynamic analysis is experimental and comparative, on account of different thermal mass, position of the cavity and geometry;

(2) the VFs are mated with a controlled ventilation system, used to parameterize the thermodynamic behavior under stepwise variations of the air inflow;

(3) temperatures and heat fluxes are predicted by means of machine learning models; and

(4) the best configuration is determined through simulations performed by means of the abovementioned machine learning models without resorting to onerous *in situ* experimentations.

The rest of the paper is structured as follows: Section 2 presents the characteristics of the test-room and the three proposed VFs and describes the sensing equipment used in the experimentation. The analysis of the collected data, the evaluation of predictive models and the discussion of the simulation results are reported in Section 3, while Section 4 draws conclusions and discusses future work.

2. Materials and methods

The purpose of the present section is to describe the experimental building and the machine learning algorithms, which were used to predict temperatures and heat fluxes under different boundary conditions.

2.1 Case study building and ventilated façade variants

The experimental study was conducted in Agugliano (Central Italy, latitude: 43.54°, longitude: 13.37°, altitude: 137 m a.s.l.). Owing to its warm and temperate climate, Agugliano falls into the Cfa class, according to the upgraded Köppen–Geiger classification (Peel *et al.*, 2007).

Agugliano has an average temperature of 15°C and an average annual rainfall of 681 mm. The hottest month is July reaching 25.1°C on average, while the coldest is January with an average temperature of 6.2°C.

The monitoring campaign lasted one month during the hottest time of the year (August 8, 2019–September 8, 2019) to verify the performance of the VFs in summertime, under intense solar exposure (see Figure 1 and Table 1).

The test-room (see Figure 2) is a windowless, uninhabited space especially engineered for research purposes. The design is carefully conceived to minimize the disturbance of chaotic phenomena and the interaction between competing phenomena (e.g. internal gains, solar gains), thus allowing to isolate the contribution of individual thermo-physical parameters. The reader is referred to Ulpiani *et al.* (2017) for an exemplary study taking advantage of the unique design features. With a net area of 12.54 m^2 and a volume equal to 36.10 m^3, the room is highly sensitive to indoor perturbations, while thanks to its hyper-insulation (U-value = 0.196 W/m^2K), it attenuates the oscillations caused by outdoor variations. The bearing structure relies on cross-laminated timber panels and is suspended at 0.4 m above the ground to minimize the heat transfer with the ground. The walls are perfectly aligned with cardinal directions and are composed by different layers as detailed in Figure 3.

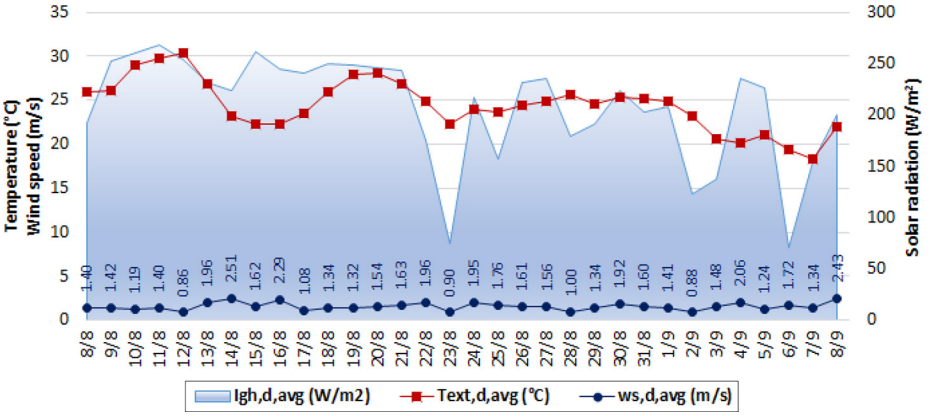

Figure 1.
Climate data of the monitored period (8 August–8 September)

Table 1.
Average, maximum and minimum values of the climatic parameters during the experimental campaign

	External temperature (°C)	Relative humidity (%)	Pressure (hPa)	Wind speed (m/s)	Global horizontal radiation (W/m^2)
average	24.2	63.7	999.4	1.3	67.3
max	27.1	73.9	1,000.2	5.5	248.3
min	22.1	49.4	998.6	0.0	0.0

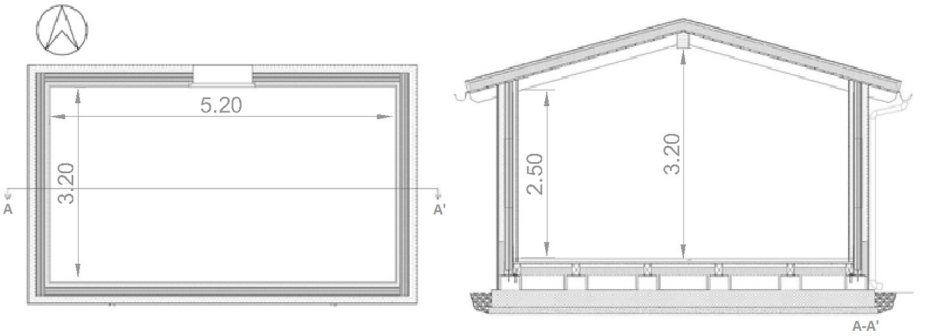

Figure 2.
Test room plan and section

The most-irradiated façade (due west) was equipped with the three ventilated skins raised 0.3 m from the ground: two massive variants of 0.8 m width and 2.3 m height and one wood-concrete blocks variant of 1 m width and 2.3 m height, built one next to the other. The two massive variants (hereinafter named EM and IM) were compared, having external or internal thermal mass with respect to the 6 cm ventilated cavity, respectively (see Figure 3). The cavity in EM was bounded by the hollow bricks layer and the external plaster (Layers 8–9 in Figure 3), whereas that in IM was bounded by the oriented strand board (OSB) panel and the external plaster (Layers 9–10 in Figure 3). The third variant was a monolayer structure, with two 3-cm-thick shells of cement-bonded wood fiber enclosing four 14-cm ventilated cavities. Having both internal and external thermal mass, this variant is

External mass (EM)	Internal mass (IM)	Internal-External mass (IEM)
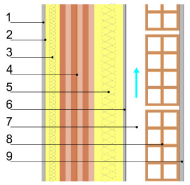	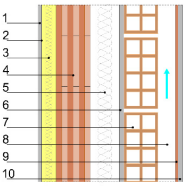	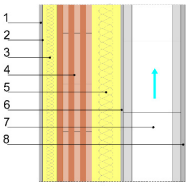
Common wall layers		
1. Internal Plasterboard (s=1.2 cm; λ=0.20 W/mK; c=0.84 kJ/kgK; φ=760 kg/m^3)		
2. Vapor barrier (s=1.0 cm; λ=0.17 W/mK; c=1.50 kJ/kgK; φ=425 kg/m^3)		
3. Internal insulation (s=5.0 cm; λ=0.04 W/mK; c=1.03 kJ/kgK; φ= 70kg/m^3)		
4. Cross laminated timber (s=12.0 cm; λ=1.4 W/mK; c=2.70 kJ/kgK; φ= 500kg/m^3)		
5. External insulation (s=10.0 cm; λ=0.036 W/mK; c=1.03 kJ/kgK; φ=90 kg/m^3)		
6. Cement mortar (s=1.0 cm; λ=0.48 W/mK; c=1.00 kJ/kgK; φ=1150 kg/m^3)		
VF layers		
7. Air cavity (s=6.0 cm; R=0.18 m^{2}K/W)	7. Hollow brick (s=12.0 cm; λ=0.35 W/mK; c=0.8 kJ/kgK; φ=750 kg/m^3)	7. Wood-concrete block with air gap (s=20.0 cm; λ*=0.103 W/mK; c*=2.0 kJ/kgK; φ*=500 kg/m^3)
8. Hollow brick (s=12.0 cm; λ=0.35 W/mK; c=0.8 kJ/kgK; φ=750 kg/m^3)	8. Air cavity (s=6.0 cm; R=0.18 m^{2}K/W)	11. External plaster (s=1.2 cm; λ=0.70 W/mK; c=1.0 kJ/kgK; φ=1000 kg/m^3)
9. External plaster (s=1.2 cm; λ=0.70 W/mK; c=1.0 kJ/kgK; φ=1000 kg/m^3)	9. OSB panel (s=0.9 cm; λ=0.13 W/mK; c=1.7 kJ/kgK; φ=650 kg/m^3)	
	10. External plaster (s=1.2 cm; λ=0.70 W/mK; c=1.0 kJ/kgK; φ=1000	

Notes: The following thermo-physical characteristics are specified:
s = thickness (cm); λ = thermal conductivity (W/mK); c = specific heat capacity (kJ/kgK); φ = density (kg/m^3); R = thermal resistance (m^{2}K/W)

Figure 3.
Composition of the walls and VF prototypes

hereinafter referred to as IEM. This system permits the construction of a VF on new buildings with a drastically reduced economic impact compared to traditional technologies. This is possible because the IEM ventilated façade is built parallel to the supporting structure with prefabricated materials (see Plate 1) [wood-concrete block and fixing system certified according to DIN EN 845-1 (Deutsches Institut für Normung, 2016)].

For each VF, the external finishing was white plasterboard, exhibiting 0.9 emissivity and 0.6 solar reflectivity. Each VFs' side was air-tightened and sealed with XPS.

Plate 1.
Wood-concrete block and fixing system (IEM VF)

The thermal properties are collected in Table 2, following standardized calculation methods, as detailed in ISO 6946:2008 (International Organization for Standardization, 2008a) and ISO 13786:2008 (International Organization for Standardization, 2008b) and assuming strongly ventilated air cavities. As such, the U-value, the surface mass, the decrement factor, the time lag and the periodic thermal transmittance were computed by excluding the thermal resistance of the air gap and all the following outer layers.

2.2 Mechanical ventilation and sensing equipment

During the campaign, different ventilation magnitudes were tested. To exert full control on the ventilation inside the cavity, an array of 13 high-speed, PWR-controlled fans was mounted on top of each VF's cavity. By changing the applied voltage within 0–10 V, the airflow could be incremented up to 67 m^3/h and the air velocity in the gap could be modulated. A variety of sensors was deployed across the ventilated walls, indoors and outdoors to monitor the thermodynamic variations, their impacts and their drivers. The network is displayed in Figures 4 and 5 and includes:

Thermal properties	VF typology EM	IM	IEM
Thermal transmittance U (W/m^2K)[a,b]	0.196	0.184	0.185
Surface mass Ms (kg/m^2)[b]	116	206	131
Decrement factor f[b]	0.096	0.053	0.072
Time lag *t* (h)[b]	12.43	16.77	15.04
Periodic thermal transmittance Y_{12} (W/m^2K)[b]	0.019	0.010	0.013

Notes: [a]Calculated according to ISO 6946:2008 (International Organization for Standardization, 2008a) U < 0.26 W/m^2K according to the Italian regulation on energy efficiency (D.M. 2015) (M. of I. E. Development, 2015). [b]Calculated according to EN ISO 13786:2008 (International Organization for Standardization, 2008b), considering a well-ventilated facade by disregarding the outer layer

Table 2.
Ventilated skins: steady state and dynamic thermal parameters

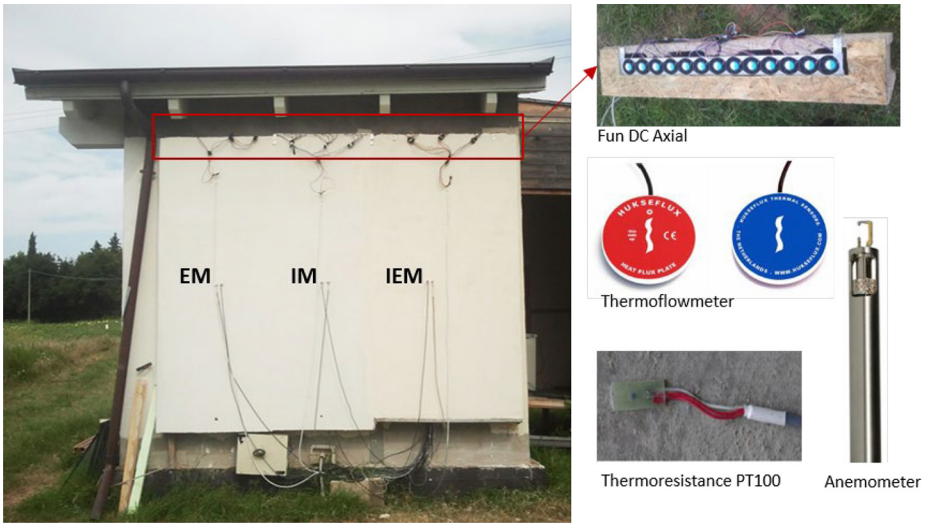

Figure 4.
Sensors used in the experimentation

- a meteorological station, located 3 m away from the western façade and measuring dry-bulb temperature, relative humidity, global solar irradiation, wind speed and wind direction;
- 12 wall-plate RTDs to measure the surface temperature of each external finishing at mid-height (115 cm above the ground) and of each internal surface overlooking the air cavity at three different heights (60 cm, 115 cm and 168 cm) on account of vertical gradients;
- wall-plate thermo-fluxmeters on the innermost side of the ventilated cavity at 115 cm height to measure the incoming (positive) and outgoing (negative) heat fluxes. One extra flux meter was used to measure the heat transfer between the IEM VF and the existing wall; and
- three hot-sphere anemometers placed inside the cavities at mid-height (115 cm) to track the kinetic energy of the airflow blown inside each VF.

The details on manufacturers, models, accuracies, ranges and time constants of the above sensors are summarized in Table 3.

The analog (input and output) signals were digitalized via sensor-specific NI-DAQ acquisition modules and processed through a Virtual Instrument coded in LabVIEW. The sampling frequency was set at the maximum (0.1 Hz). As a first trial, we aimed at imposing a PID feedback control on the air velocity inside the cavities by modulating the voltage to the arrays of fans individually. The dynamicity of the process turned out to exceed the sampling frequency, thus resulting in untimely and offsetted control actions. It was therefore decided to apply a daily voltage variation (from 0 to 10 V) (see Figure 6) to collect a parameterized data set, refined enough to conduct multivariate regression analysis through

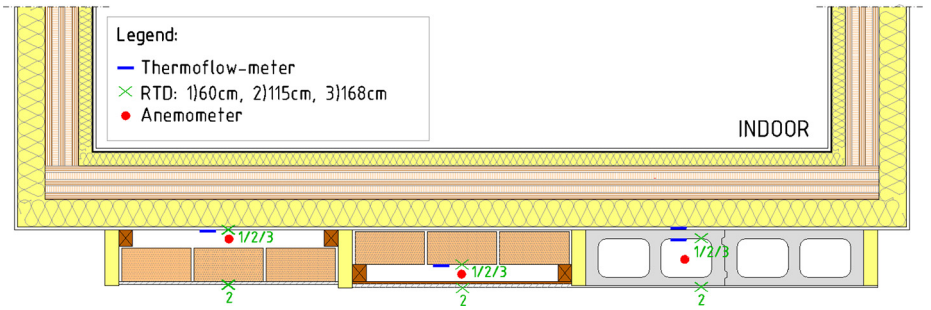

Figure 5.
Distribution of anemometers, RTDs and thermoflux-meters

Measure	Sensor type	Model	Range	Accuracy
Meteorological station				
Air temperature	Thermo hygrometer	DMA875	−30°C to +70°C	0.05°C
Relative humidity	Thermo hygrometer	DMA876	0 to 100%	0.25%
Atmospheric pressure	Piezoelettric	DQA	800 to 1,100 hPa	0.5 hPa
Wind velocity	Anemometer	WMT700	0 to 75 m/s	/
Wind direction	Anemometer	WMT700	0 to 270°	/
Solar radiation	Radiometer	DPA153	0 to 2,000 W/m^2	<5%
Wall sensors				
Surface temperature	Platinum resistor	PT 100	−40°C to +80°C	0.05°C
Heat flux	Heat flow meter	HFP01	−2,000 to +2,000 W/m^2	2%
Air velocity	Anemometer	ESV107	0,01 ÷ 20 m/s	0.03 m/s

Table 3.
Information about the sensors used in the experimental study

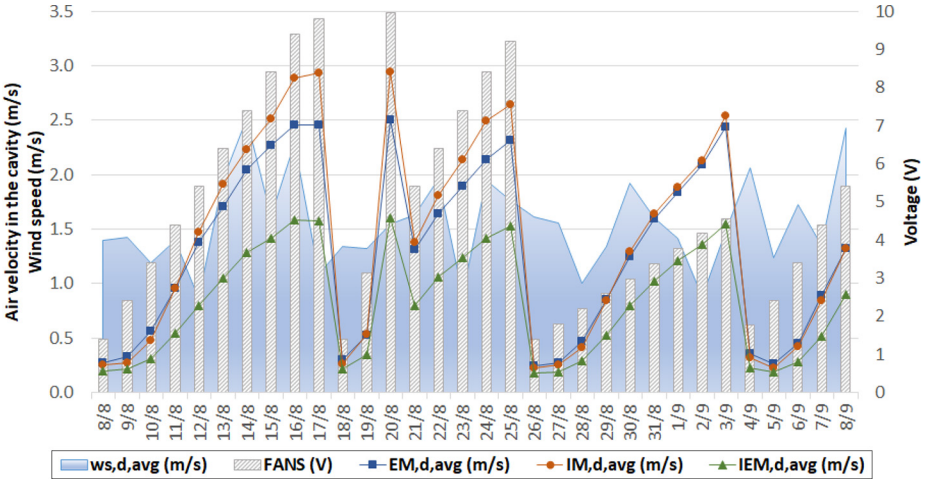

Figure 6.
Average daily air speed in the cavity as a function of the selected voltage and daily average wind speed

machine learning algorithms. The goal of the analysis was to forecast surface temperatures and thermal fluxes for the three considered VFs by using meteorological data and air velocity in the cavity as predictive variables. A detailed description of the experimentation is presented in the next section.

2.3 Experimental setup

The data set collected in the experimentation consists of 283,072 samples corresponding to measurements performed in the interval August 8, 2019–September 8, 2019 with a sampling rate of 0.1 Hz. Each sample contains measurements related to all three considered VFs in terms of:

(1) meteorological measurements (common to all VFs): external temperature, humidity, pressure, irradiance, wind speed and direction;

(2) VF-specific measurements: air velocity, surface temperature at three different heights (0.60, 1.15 and 1.68 m), external temperature and heat flux; and

(3) timestamp of the measurements.

Three regression algorithms were evaluated for the prediction of surface temperatures and thermal fluxes for the three VFs. In particular, two traditional machine learning algorithms and a deep learning algorithm were considered. For what concerns the former category of algorithms, the regression tree (RT) (Breiman *et al.*, 1983) and the support vector regression (SVR) (Drucker *et al.*, 1997) algorithms, which, respectively, represent variants of decision tree (Safavian and Landgrebe, 1991) and support vector machine (Cortes and Vapnik, 1995) for continuous target variables, were evaluated.

The RT algorithm is based on an iterative process that splits the data into partitions by defining a condition on a single feature at a time and then continues splitting each partition into smaller groups as the algorithm passes through each branch until each node reaches a user-specified minimum node size and becomes a terminal node (also called leaf node). The set of conditions defined on features is used to define an appropriate line that fits the data.

The SVR algorithm estimates a regression function by determining the function f that minimizes the number of data samples that are at a distance lower than a user-defined parameter ε from f.

The versions of RT and SVR used in this work are available in Rapidminer (2022).

With respect to deep learning algorithms, the long short-term memory (LSTM) algorithm (Hochreiter and Schmidhuber, 1997), which is a recurrent neural network that can learn long-term dependencies among sequential data, was considered. The LSTM network contains cycles that feed the network activations from a previous time step as new inputs to the network to influence predictions at the current time step. These activations are stored in the internal states of the network which can, in principle, hold long-term temporal contextual information. This mechanism allows RNNs to exploit a dynamically changing contextual window over the input sequence [44]. LSTM was implemented using the Keras framework [45], which offers high-level application programming interfaces (APIs) for designing deep learning algorithms in Python.

A different regression model was built for each target variable of each VF:

- EM: T1_60, T1_115, T1_168, T1_ext, Flux1
- IM: T2_60, T2_115, T2_168, T2_ext, Flux2
- IEM: T3_60, T3_115, T3_168, T3_ext, T3_int, Flux3, Flux4

where the target variable Tn_y represents the temperature measured in the n-th VF at height y, Tn_ext is the external temperature and Fluxn is the heat flux measured in the n-th VF, respectively. The n values 1, 2 and 3/4 are attributed to EM, IM and IEM, respectively. As already mentioned in Section 2.2, two different heat fluxes and the internal temperature were considered in the IEM variant.

All the other measurements (meteorological measurements, air velocity and timestamp) were considered as features for our regression models.

The performance of regression models was evaluated by means of the root-mean-square error (RMSE), which is defined as $RMSE = \sqrt{\frac{\sum_{i=1}^{N} (y_i - x_i)^2}{N}}$, where x_i is the predicted value and y_i is the true (i.e. measured) value.

The generalizability of discovered models was evaluated by performing a 10-fold cross validation; the results reported in the next subsection are the averages of the 10 folds. Parameter tuning of the algorithms was performed by testing different parameters' values and choosing the values that gave the best result, namely, minimal average RMSE. In particular, the ranges for each algorithm were as follows:

- RT: maximal depth $d \in [1,15]$ and minimum number of samples for each node (i.e. leaf size) $l \in [1, 10000]$ with 16 linear steps. Each experiment was repeated both in the presence and in the absence of pruning techniques ($p \in$ [true, false]), with the aim of evaluating the effects of pruning in reducing overfitting;
- SVR: the dot kernel was used and the algorithm was trained for a maximum number of iterations $i \in [20, 20000]$ with 10 linear steps by also varying the cost parameter $C \in [0, 5]$ with 10 linear steps and the maximum error $\varepsilon \in [0.00001, 4]$ with 10 steps; and
- LSTM: a single-layer architecture was tested with a variable number of units $n \in \{5, 10, 20, 50, 70, 100\}$ and epochs $e \in \{5, 10, 20, 50, 100, 200, 500\}$.

A total of 17 (target variables) × 1,917 (different configurations of algorithms) × 10 (folds) = 325,890 experiments was performed. Results are reported in Section 3.

3. Experiments

The goal of the experimentation was twofold: building an accurate regression model for each target variable and assessing the impact of the variation of each feature on the performance of regression models, i.e. the relative feature weights.

For what concerns the first goal, Table 4 reports the results of the best regression model for each target variable and regression algorithm. The value of the pruning parameter of the RT and the maximum number of iterations of the SVR are omitted since they are constant among all the best models and are respectively equal to "true" and 8012.

It can be noticed that surface temperatures are better predicted by the RT, while LSTM performs better on heat fluxes. In no case SVR models result to be the best predictors. As a general consideration, surface temperatures seem to be predicted more accurately than fluxes: it may be explained by the more dynamic nature of heat fluxes, whose values may be altered by turbulences, thus being more challenging to predict.

It can also be noticed that the prediction of external surface temperatures is less accurate than that of the other surface temperatures, as RMSE is usually higher. In fact, a lower RMSE is related to a higher prediction accuracy.

Small differences can be appreciated among VFs: in particular, regression models for VF2 have the minimum prediction error for what concerns surface temperatures, even if differences with other VFs are negligible (<0.1°C).

On the contrary, models for VF2 show the worst performance in predicting heat fluxes, with RMSE 12 times higher than that obtained for VF1. For what concerns LSTM models, it can be observed that models with a high number of epochs and a small number of units exhibit the best performance.

Regression models for surface temperatures are affected by low prediction errors (RMSE < 0.272°C), while errors for heat fluxes are excessively high compared to the range of measured values. Hence, the proposed machine learning techniques seem to be able to accurately capture the physical phenomenon only in the case of temperatures.

The second goal of the experimentation was the evaluation of feature weights for each target variable. In particular, the focus was on determining the physical quantities more strongly related to the prediction of surface temperatures, namely, linked to the best prediction performance. To this end, the best-performing models obtained by RT were used since this algorithm allows for an explicit analysis of feature weights. In particular, at each iteration, the feature that minimizes the sum of squares between the actual value and the mean in each of its children nodes is selected (least squares criterion). The improvement due to each feature is used to compute its weight.

Relative weights, normalized in the range [0, 1], are reported in Table 5. In case of T1_ext, T2_ext and T3_ext, the air velocity inside the VFs' cavities has not been considered since it is not related to such measurements.

Generally speaking, the variation of air velocity, the temperature and the air humidity seem to have a higher impact on the prediction of surface temperatures with respect to other physical quantities. As expected, temperature typically plays a major role (weights: $0.227 \div 0.474$) while wind direction and speed contribute marginally (<0.1).

The coherence between the features chosen by the model as most significant and those expected to be more relevant from the knowledge of the physical phenomenon (Rahiminejad and Khovalyg, 2021) provides further proof of the reliability of the model.

4. Results and discussion

4.1 Energy performance analysis

As already discussed in Section 2.2, the air velocity inside the cavity cannot be kept constant through PID-controlled fans due to the high dynamicity of the process. For this reason, the regression models described in the previous section were used to predict the surface temperatures of the cavity by using meteorological data and constant, predefined values for air velocity in the cavity as inputs. In particular, the air velocity was varied in the

Variable	RT	SVR	LSTM	Variable	RT	SVR	LSTM
T1_60	0.272	1.186	0.486	T3_115	0.234	1.273	0.469
	(d = 14, l = 1)	(C = 0, ε = 1)	(n = 5, e = 500)		(d = 15, l = 1)	(C = 0, ε = 1)	(n = 5, e = 500)
T1_115	0.269	1.277	0.502	T3_168	0.232	1.068	0.459
	(d = 15, l = 1)	(C = 0, ε = 1)	(n = 10, e = 500)		(d = 15, l = 1)	(C = 0, ε = 1)	(n = 5, e = 500)
T1_168	0.229	1.334	0.431	T3_ext	0.724	3.858	1.164
	(d = 15, l = 1)	(C = 0, ε = 1)	(n = 5, e = 500)		(d = 15, l = 1)	(C = 0, ε = 2.5)	(n = 20, e = 500)
T1_ext	0.579	3.161	1.804	T3_int	0.235	1.167	0.396
	(d = 15, l = 1)	(C = 0, ε = 2.125)	(n = 20, e = 500)		(d = 15, l = 1)	(C = 0, ε = 0.001)	(n = 20, e = 500)
T2_60	0.198	1.297	0.411	Flux1	0.929	2.448	0.206
	(d = 15, l = 1)	(C = 0, ε = 1)	(n = 5, e = 500)		(d = 13, l = 650)	(C = 0, ε = 2.875)	(n = 5, e = 500)
T2_115	0.189	1.462	0.428	Flux2	3.814	36.512	2.586
	(d = 15, l = 1)	(C = 0, ε = 1)	(n = 5, e = 500)		(d = 14, l = 1)	(C = 0, ε = 1)	(n = 5, e = 500)
T2_168	0.196	1.503	0.394	Flux3	2.277	33.029	1.426
	(d = 15, l = 1)	(C = 0, ε = 1)	(n = 5, e = 500)		(d = 12, l = 1)	(C = 0, ε = 1.375)	(n = 5, e = 500)
T2_ext	0.707	4.063	0.946	Flux4	1.055	13.871	0.322
	(d = 15, l = 1)	(C = 0, ε = 2.215)	(n = 5, e = 500)		(d = 9, l = 1)	(C = 0, ε = 2.5)	(n = 20, e = 500)
T3_60	0.226	1.032	0.421				
	(d = 15, l = 1)	(C = 0, ε = 1)	(n = 10, e = 500)				

Table 4.
RMSE of the best regression model for each target variable (parameter values are indicated in round brackets under the RMSE)

interval [0, 4] m/s with step 0.2 m/s and experiments for each combination of air velocity, VF and surface temperature were performed. The goal was to identify the lowest average surface temperatures for each VF.

The results show that the inducted models are able to accurately forecast temperatures only for air velocity values which appear in at least 2,000 samples of the initial data set. On the basis of such hypothesis, a frequency analysis was conducted to evaluate acceptable values for each VF. As shown in Figure 7, only velocities in [0.2, 2.8] m/s for EM, in [0.2, 3.2] m/s for IM and [0.2, 1.8] m/s for IEM were considered.

The results of the experimentation with the RT models are reported in Figures 8, 9 and 10.

In Figures 8 and 9, the VFs EM and IM show a similar trend as air velocity in the cavity varies. In fact, both have low-temperature values at 0.2 m/s, probably due to the increase in thermal resistance caused by the almost stationary air layer. Such hypothesis is supported by the fact that cavities usually used in buildings typically add a thermal resistance of 0.16 m^2K/W in case of cover floors and 0.18 m^2K/W in case of façades [46]. Also, in both VFs, when the air velocity equals 0.4 m/s, an increase in temperature of about 0.5°C is observed

Table 5.
Relative weights for each target variable of air velocity (AV) inside the cavity, air temperature (at), relative humidity (RH), solar irradiance (SI), atmospheric pressure (AP), wind direction (WD) and wind speed (WS)

Variable	AV	AT	RH	SI	AP	WD	WS
T1_60	0.249	0.227	0.140	0.125	0.093	0.082	0.082
T1_115	0.260	0.228	0.139	0.119	0.098	0.071	0.083
T1_168	0.235	0.357	0.146	0.093	0.072	0.041	0.055
T1_ext	==	0.474	0.184	0.107	0.101	0.053	0.081
T2_60	0.225	0.359	0.138	0.098	0.077	0.044	0.060
T2_115	0.227	0.378	0.127	0.102	0.069	0.039	0.056
T2_168	0.245	0.350	0.143	0.101	0.071	0.040	0.048
T2_ext	==	0.377	0.194	0.145	0.103	0.080	0.099
T3_60	0.244	0.261	0.145	0.118	0.091	0.062	0.079
T3_115	0.231	0.365	0.138	0.092	0.073	0.042	0.058
T3_168	0.242	0.361	0.140	0.086	0.074	0.040	0.055
T3_ext	==	0.417	0.194	0.130	0.101	0.072	0.085
T3_int	0.227	0.389	0.131	0.091	0.073	0.039	0.049

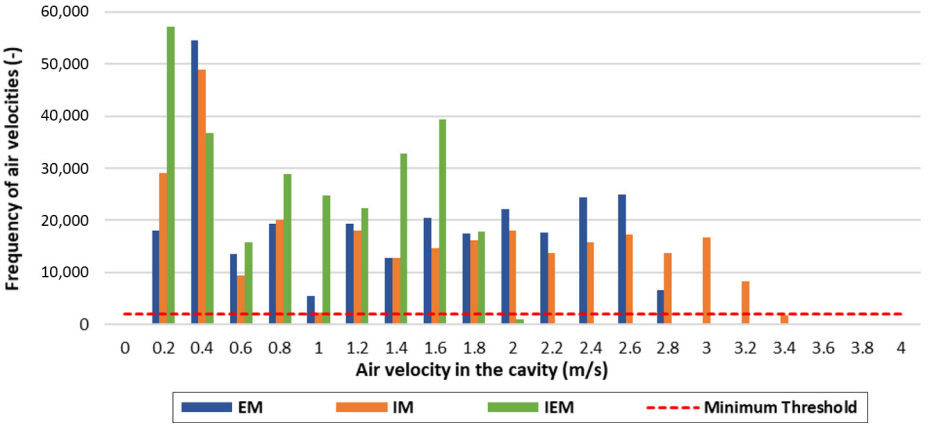

Figure 7.
Frequency analysis of air velocities in the three VFs. The "Minimum Threshold" represents the threshold of air velocity inside the cavity, below which predictive models fail to accurately estimate surface temperatures

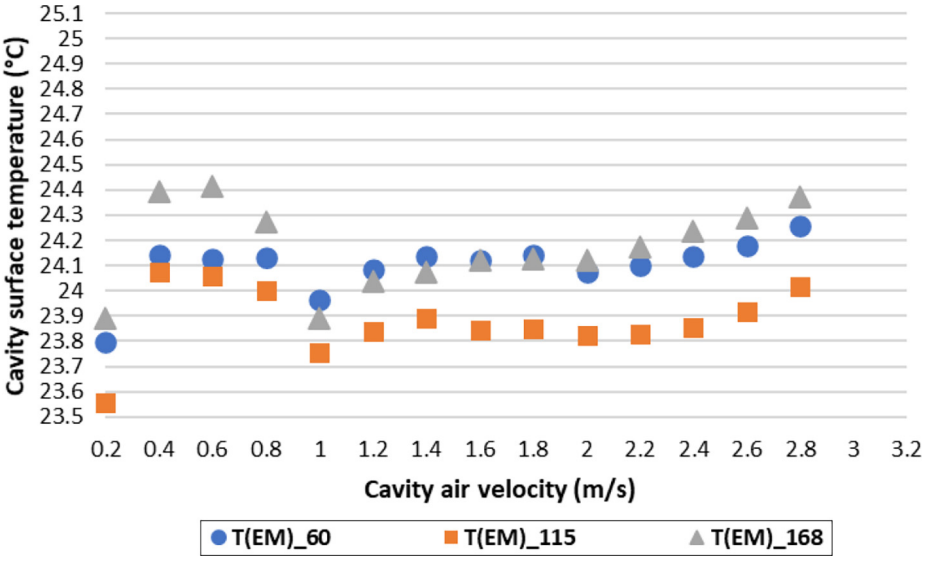

Figure 8. Predictions of cavity surface temperatures for the EM wall as a function of air velocity

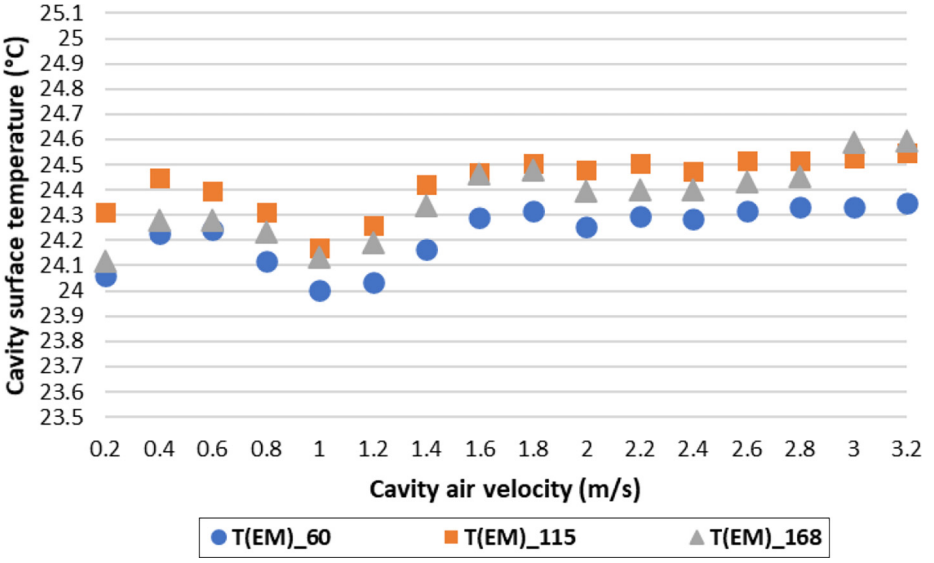

Figure 9. Predictions of cavity surface temperatures for the IM wall as a function of air velocity

for the EM façade and of 0.2°C for the IM façade, most likely caused by the intake of warm external air in the cavity (increased heat exchange by conduction) and a weak convective heat exchange.

Besides 0.2 m/s, the velocity of 1 m/s seems to be the one that minimizes the surface temperatures for both the EM and IM façades. This velocity value seems to represent a good compromise between convective and conductive heat exchange. Above 1 m/s, temperatures

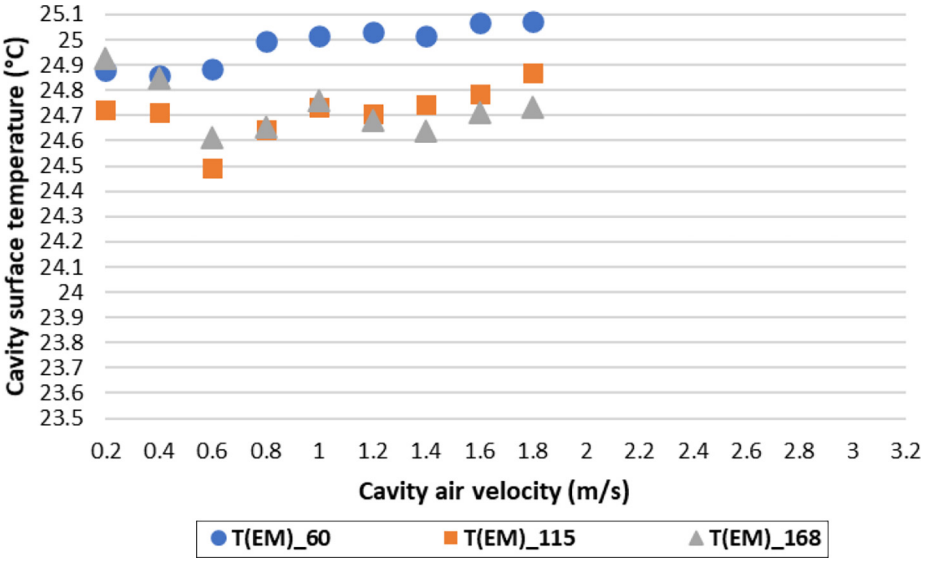

Figure 10.
Predictions of cavity surface temperatures for the IEM wall as a function of air velocity

start to rise again as the air in a highly ventilated cavity is at about the same temperature as the external air (Cened, 2011).

In contrast, the IEM's surface temperature appears to hit its absolute minimum at a speed of 0.6 m/s (see Figure 10). In general, the air velocities reached inside the cavity are lower than those recorded in the other VFs owing to the greater roughness of the surfaces that delimit the cavity and the larger thickness of the cavity itself (16 cm). It can also be noted that, in the IEM wall, the vertical temperature gradient is more accentuated than in the other design variants. In absolute terms, the lowest surface temperature value is the one predicted at 115 cm for the VF EM (23.6°C at 0.2 m/s), while the IEM at 60 cm reaches the highest value (25.1°C at 1.8 m/s).

From the analysis of the experimental results, it can be concluded that the increase in air velocity in VFs' cavities does not necessarily lead to an advantage in terms of surface temperatures (and hence of heat fluxes). Instead, there are minima at specific velocities: 1 m/s for the VF EM and IM and 0.6 m/s for the IEM. It is also evident that the IEM wall is the worst-performing from an energy perspective, while the EM is the best-performing.

In Figures 11 and 12, the surface temperature difference between a wall with and without a ventilated façade is represented. In both figures, the temperatures refer to the sensor placed at 115 cm on the wall in contact with the internal environment, so in the case of the three VFs, they refer to the surface temperatures of the cavities (as specified in Figure 5), while the surface temperature of the wall without VF refers to the surface in contact with the external air. Only the simulations related to the optimal velocities inside each cavity (1 m/s for EM and IM and 0.6 m/s for IEM) are taken into consideration. In particular, it can be observed that VFs are more effective at high solar radiation values (Gagliano and Aneli, 2020) (see Figure 11), resulting in a decrease in average surface temperature of 3.6°C, up to a maximum of 12.4°C.

When the radiation is low or nonexistent, i.e. at night or on cloudy days (see Figure 12), the VFs do not seem to provide a beneficial contribution to the building's thermal balance,

with an average increase in surface temperatures of 1.3°C and a maximum of 4.9°C. It must be noticed, however, that the negative effect of the increase in surface temperatures at night, and thus the increase in heat flow to the air-conditioned space, is three times less than the benefit that VFs provide on extremely bright days. In addition, the increase in night heat flow (conductive exchange) can be compensated by free cooling ventilation (convective exchange) (Rey-Hernández *et al.*, 2019).

Under stationary conditions, the heat flux per unit area is calculated by equation (1):

$$\dot{q} = \frac{Q}{A \cdot t} = U \cdot (T_1 - T_2) W/\mathrm{m}^2 \quad [1]$$

where:

Q is the quantity of heat exchanged (J), A is the exchange surface (m^2), t is the time (s), U is the thermal transmittance (W/m^2K), T_1 is the surface temperature of the warmest facade (°C) and T_2 is the surface temperature of the coldest facade (°C).

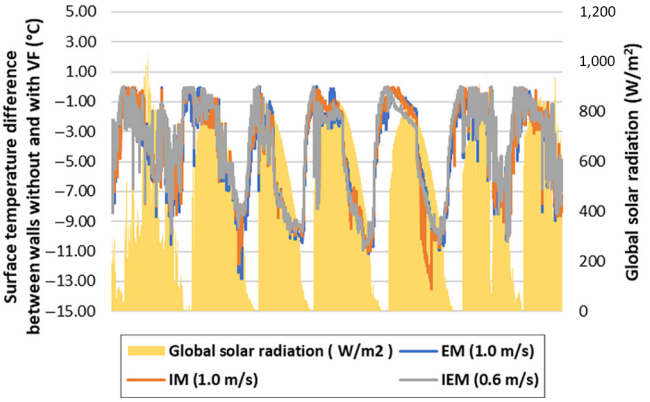

Figure 11.
Difference of surface temperatures between walls with and without VF in relation to global solar radiation. Negative differences indicate lower surface temperatures in the presence of VFs

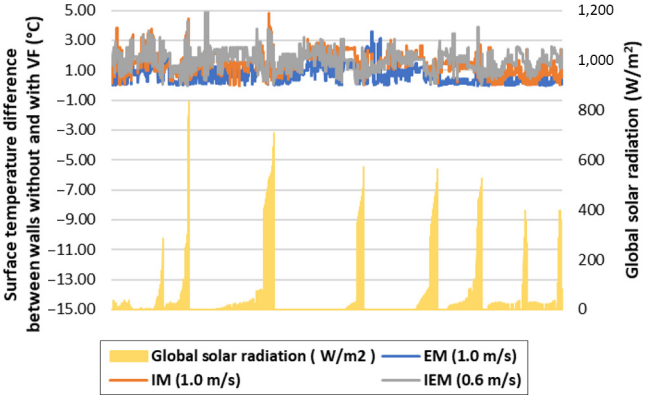

Figure 12.
Difference of surface temperatures between walls with and without VF in relation to global solar radiation. Positive differences indicate higher surface temperatures in the presence of VFs

Assuming a surface temperature inside the thermal zone of 26°C, the heat flux per unit area increases to 128.93% for the wall without a ventilated façade compared to the EM (see Table 6).

4.2 Cost assessment

Cost analysis was performed by only considering the cost of the three VFs, as the wall behind the three ventilated structures, the external plaster and the steel supports are the same for all variants. The cost of the structures was extracted from the Italian national price list (DEI Tipografia del Genio Civile, 2021), which results from an in-depth market survey concerning materials, hourly costs, machinery and equipment, labor and safety works. With reference to the stratigraphies listed in Figure 2, the costs of the following materials were identified (see Table 7):

In terms of cost, the best ventilated façade is the EM, which has also proven to be the best variant from an energy perspective in the analysis performed in Section 4.1.

5. Conclusions

The thermo-hydrodynamic behavior of the air inside the cavities of ventilated facades is extremely complex and influenced by many factors such as external and internal climatic conditions, cladding materials, thermo-physical and geometrical properties of the wall. Theoretical calculations, numerical analysis and CFD simulations can help determining the air flow rate in ventilated cavities, but some physical phenomena are difficult to capture or implement. For this reason, in some research works, the authors provide experimental measurements to support the simulation results, which, however, present maximum air velocity values in the cavity of 1 m/s (for brick, concrete, wood and ceramic cladding) (Rahiminejad and Khovalyg, 2021) and therefore do not represent a sufficient pool of data to verify all simulated cases.

In this work, to achieve higher cavity air velocities than those described in the literature, a forced mechanical ventilation system was integrated with the VFs, reaching velocities up to 3.2 m/s.

Table 6.
Heat flow for unit area of walls with and without VF

	EM	IM	IEM	no VF
U (W/m^2K)	0.20	0.18	0.19	0.20
T_{int} (°C)	26.00	26.00	26.00	26.00
T_{ext} (°C)	28.98	29.21	29.54	32.83
q (W/m^2)	0.58	0.59	0.66	1.34
Δq (%)	–	0.88%	12.07%	128.93%

Table 7.
Cost of materials used for the three VF prototypes

Materials	Cost
1) Wood-concrete blocks for external and internal load-bearing walls without insulation, H-shaped, with a density of 510 ± 10% kg/m^3 and thickness of 20 cm	36.6 €/m^2
2) Brick masonry with 15 holes (12 × 25 × 25 cm) with cement and sand mortar	8.25 €/m^2
3) Oriented Strand Board (OSB), 0.9 cm thick	6.05 €/m^2

Determining the optimal air velocities and airflow rates within the cavities of the different walls makes it possible to limit heat fluxes and thus save energy in the building.

For this reason, three variants of VFs (i.e. EM, IM and IEM) were introduced and a new cost-effective approach based on machine learning techniques was defined, which allows to identify the optimal velocities by simulating temperatures and heat flows for each proposed wall configuration while avoiding the errors that could be made using theoretical calculations, numerical analysis or CFD simulations.

In particular, three different regression algorithms (i.e. RT, support vector machine for regression and LSTM) were evaluated, and it resulted that the RT outperforms all other models in case of temperatures, while heat fluxes are better predicted by LSTM networks. Generally speaking, the obtained predictive models have a remarkable accuracy in predicting temperatures, while accuracies are lower in case of heat fluxes.

The work also focused on the weight analysis of the features to determine which parameters among air velocity inside the cavity, air temperature, relative humidity, solar irradiance, atmospheric pressure, wind direction and wind speed are the most influential for the calculation of surface temperatures. On average, air temperature and air velocity inside the cavity seem to have a greater impact on the prediction of surface temperatures than the other physical quantities (32.1% and 24.0%, respectively). Relative humidity and solar radiation, on the other hand, exhibit a milder influence on the prediction (14.1% and 10.4%), while atmospheric pressure and wind speed and direction seem to be almost irrelevant. The results obtained are consistent with trends and associations documented in literature.

Using the models created for the three VFs, the optimum air velocity in each cavity was also determined to achieve the lowest surface temperature. From the simulations, it was observed that the EM and IM VFs exhibited an optimum velocity of 1 m/s, while the IEM VF was found to have an optimum velocity of 0.6 m/s. In addition, the EM wall was identified as the best variant both from an energy and economic point of view.

Finally, the heat fluxes per unit area were calculated, and it was found that the presence of a ventilated façade is able to decrease the value of the heat flux by up to 129% as compared to a non-ventilated façade with consequent energy savings.

As future direction of research, further regression algorithms will be considered, in particular for the prediction of heat fluxes. Moreover, the *in situ* data gathering will be extended to the winter season to predict the VFs' energy performance under different weather conditions. The availability of data related to a wider temporal window will also allow for the evaluation of the generalizability of the selected regression models since it is well-known that the accuracy of such models tends to decrease the more the data are different from those used for training.

Finally, additional design variants for VFs will be developed to determine their optimal velocities and best configuration.

References

Aelenei, L.E., Rodrigues, A.M. and de Lisboa, U.T. (2005), "Thermal performance of naturally ventilated cavity walls".

Aznar, F., Echarri, V., Rizo, C. and Rizo, R. (2018), "Modelling the thermal behaviour of a building facade using deep learning", *PLoS One*, Vol. 13 No. 12, p. e0207616.

Bassett, M.R. and McNeil, S. (2005), "Drained and vented cavity walls: measured ventilation rates", *IRHACE Conference. Branz*.

Bikas, D., Tsikaloudaki, K., Kontoleon, K.J., Giarma, C., Tsoka, S. and Tsirigoti, D. (2017), "Ventilated facades: requirements and specifications across Europe", *Procedia Environmental Sciences*, Vol. 38, pp. 148-154, doi: 10.1016/j.proenv.2017.03.096.

Breiman, L., Friedman, J., Olshen, R. and Stone, C.J. (1983), *Classification and Regression Trees*, Brooks/Cole Publishing, Monterey.

Cabeza, L.F., Castellon, C., Nogues, M., Medrano, M., Leppers, R. and Zubillaga, O. (2007), "Use of microencapsulated PCM in concrete walls for energy savings", *Energy and Buildings*, Vol. 39 No. 2, pp. 113-119.

Cened (2011), "Concetti di base: fisica delle pareti", Manuale CENED+ – Vers. 1.2.

Ciampi, M., Leccese, F. and Tuoni, G. (2003), "Ventilated facades energy performance in summer cooling of buildings", *Solar Energy*, Vol. 75 No. 6, pp. 491-502, doi: 10.1016/j.solener.2003.09.010.

Cortes, C. and Vapnik, V. (1995), "Support-vector networks", *Machine Learning*, Vol. 20 No. 3, pp. 273-297.

DEI Tipografia del Genio Civile (2021), "Prezzi informativi dell'edilizia", Recupero ristrutturazioni manutenzione. Ottobre.

Deutsches Institut für Normung (2016), "DIN EN 845-1 specification for ancillary components for masonry – Part 1: Wall ties, tension straps, hangers and brackets".

Drucker, H., Burges, C.J., Kaufman, L., Smola, A. and Vapnik, V. (1997), "Support vector regression machines", *Adv. Neural Inf. Process. Syst*, Vol. 9, pp. 155-161.

European Parliament (2012), "Directive 2012/27/EU of the European parliament and of the council of 25 October 2012 on energy efficiency, amending directives 2009/125/EC and 2010/30/EU and repealing directives 2004/8/EC and 2006/32/EC", Off. J. Eur. Union. 10.3000/19770677.L_2012.315.eng

European Parliament (2018), "Energy. Topics: energy efficiency", Buildings [WWW Document].

European Parliament and Council of the European Union (2018), "Directive (EU) 2018/844 of the European parliament and of the council of 30 May 2018 amending directive 2010/31/EU on the energy performance of buildings and Directive 2012/27/EU on energy efficiency", Off. J. Eur. Union 30 May, pp. 1-17.

Falk, J. and Sandin, K. (2013a), "Ventilated rainscreen cladding: a study of the ventilation drying process", *Building and Environment*, Vol. 60, pp. 173-184, doi: 10.1016/j.buildenv.2012.11.015.

Falk, J. and Sandin, K. (2013b), "Ventilated rainscreen cladding: measurements of cavity air velocities, estimation of air change rates and evaluation of driving forces", *Building and Environment*, Vol. 59, pp. 164-176, doi: 10.1016/j.buildenv.2012.08.017.

Francés, V.M.S., Escriva, E.J.S., Ojer, J.M.P., Bannier, E., Soler, V.C. and Moreno, G.S. (2013), "Modeling of ventilated façades for energy building simulation software", *Energy and Buildings*, Vol. 65, pp. 419-428.

Gagliano, A. and Aneli, S. (2020), "Analysis of the energy performance of an opaque ventilated façade under winter and summer weather conditions", *Solar Energy*, Vol. 205, pp. 531-544, doi: 10.1016/j.solener.2020.05.078.

Gagliano, A., Nocera, F. and Aneli, S. (2016), "Thermodynamic analysis of ventilated façades under different wind conditions in summer period", *Energy and Buildings*, Vol. 122, pp. 131-139, doi: 10.1016/j.enbuild.2016.04.035.

Gholamibozanjani, G. and Farid, M. (2020), "Peak load shifting using a price-based control in PCM-enhanced buildings", *Solar Energy*, Vol. 211, pp. 661-673.

Hochreiter, S. and Schmidhuber, J. (1997), "Long short-term memory", *Neural Computation*, Vol. 9 No. 8, pp. 1735-1780.

Ibañez-Puy, M., Vidaurre-Arbizu, M., Sacristán-Fernández, J.A. and Martín-Gómez, C. (2017), "Opaque ventilated façades: thermal and energy performance review", *Renewable and Sustainable Energy Reviews*, Vol. 79, pp. 180-191, doi: 10.1016/j.rser.2017.05.059.

International Organization for Standardization (2008a), "ISO 6946:2008 building components and building elements – Thermal resistance and thermal transmittance – Calculation method",

International Organization for Standardization (2008b), "ISO 13786:2008 thermal performance of building components – Dynamic thermal characteristics – Calculation methods".

Kenisarin, M. and Mahkamov, K. (2007), "Solar energy storage using phase change materials", *Renewable and Sustainable Energy Reviews*, Vol. 11 No. 9, pp. 1913-1965.

Kumar, S., Singh, M.K., Mathur, A., Mathur, S. and Mathur, J. (2018), "Thermal performance and comfort potential estimation in low-rise high thermal mass naturally ventilated office buildings in India: an experimental study", *Journal of Building Engineering*, Vol. 20, pp. 569-584.

Lorente, S. and Mattias, E. (1998), "Protection against solar over heatings using high aspect ratio open vertical cavities", *World Renewable Energy Congress. Florence*, pp. 20-25.

M. of I. E. Development (2015), "Interministerial decree of 26 June 2015 – Application of calculation methods for energy performance and definition of minimum building requirements", Gazz.

Marinosci, C., Semprini, G. and Morini, G.L. (2014), "Experimental analysis of the summer thermal performances of a naturally ventilated rainscreen façade building", *Energy and Buildings*, Vol. 72, pp. 280-287, doi: 10.1016/j.enbuild.2013.12.044.

Meir, I.A. and Roaf, S.C. (2002), "Thermal comfort–thermal mass: housing in hot dry climates", *Indoor Air*, Vol. 2, pp. 1050-1055.

Patania, F., Gagliano, A., Nocera, F., Ferlito, A. and Galesi, A. (2010), "Thermofluid-dynamic analysis of ventilated facades", *Energy and Buildings*, Vol. 42 No. 7, pp. 1148-1155, doi: 10.1016/j.enbuild.2010.02.006.

Peel, M.C., Finlayson, B.L. and McMahon, T.A. (2007), "Updated world map of the Köppen-Geiger climate classification", *Hydrol. Earth Syst. Sci. Discuss*, Vol. 4, pp. 439-473.

Piñon, J.P., Burnett, E.F.P., Davidovic, D. and Srebric, J. (2004), "The airflow characteristics of ventilated cavities in screen-type enclosure wall systems (RP-1091)", Therm. Perform. Exter. Envel. Whole Build.

Rahiminejad, M. and Khovalyg, D. (2021), "Review on ventilation rates in the ventilated air-spaces behind common wall assemblies with external cladding", *Building and Environment*, Vol. 190, p. 107538, doi: 10.1016/j.buildenv.2020.107538.

Rapidminer (2022), available at: https://rapidminer.com

Rey-Hernández, J.M., González, S.L., San José-Alonso, J.F., Tejero-González, A., Velasco-Gómez, E. and Rey-Martínez, F.J. (2019), "Smart energy management of combined ventilation systems in a nZEB", *E3S Web of Conferences*, Vol. 111, doi: 10.1051/e3sconf/201911101050.

Safavian, S.R. and Landgrebe, D. (1991), "A survey of decision tree classifier methodology", *IEEE Transactions on Systems, Man, and Cybernetics*, Vol. 21 No. 3, pp. 660-674.

Sha, H., Moujahed, M. and Qi, D. (2021), "Machine learning-based cooling load prediction and optimal control for mechanical ventilative cooling in high-rise buildings", *Energy and Buildings*, Vol. 242.

Stazi, F., Ulpiani, G., Pergolini, M., Di Perna, C. and D'Orazio, M. (2020), "The role of wall layers properties on the thermal performance of ventilated facades: experimental investigation on narrow-cavity design", *Energy and Buildings*, Vol. 209, doi: 10.1016/j.enbuild.2019.109622.

Straube, J. and Finch, G. (2007), "Ventilated wall claddings: review, field performance, and hygrothermal modeling",

Ulpiani, G., Giuliani, D., Romagnoli, A. and di Perna, C. (2017), "Experimental monitoring of a sunspace applied to a NZEB mock-up: assessing and comparing the energy benefits of different configurations", *Energy Build*, Vol. 152, doi: 10.1016/j.enbuild.2017.04.034.

Vanpachtenbeke, M., Langmans, J., Van den Bulcke, J., Van Acker, J. and Roels, S. (2017), "On the drying potential of cavity ventilation behind brick veneer cladding: a detailed field study", *Building and Environment*, Vol. 123, pp. 133-145, doi: 10.1016/j.buildenv.2017.06.047.

Van Straaten, R., Straube, J., Trainor, T. and Habellion, A. (2016), "Wind washing effects on mineral wool insulated sheathings", *Proc. Build. XIII*.

Further reading

Keras (2022), available at: https://keras.ic

Corresponding author

Alex Mircoli can be contacted at: a.mircoli@univpm.it